Electronic Supplementary Material (ESI) for Chemical Science.
This journal is © The Royal Society of Chemistry 2019

Supporting information

# Symbiotic hetero-nanocomposite that stabilizes unprecedented $CaCl_2$-type $TiO_2$ for enhanced solar-driven hydrogen evolution reaction

*Yuelan Zhang,*[a] *Liping Li,*[*a] *Yan Liu,*[a] *Tao Feng,*[a] *Shibo Xi,*[b] *Xiyang Wang,*[a] *Chenglin Xue,* [a] *Jingyu Qian,*[c] *Guangshe Li*[*a]

[a] States Key Laboratory of Inorganic Synthesis and Preparative Chemistry, College of Chemistry, Jilin University, Changchun 130012, P.R. China

[b] Institute of Chemical and Engineering Sciences, A*STAR, 1 Pesek Road, Jurong Island, Singapore 627833, Singapore

[c] State Key Laboratory of Supramolecular Structure and Materials, College of Chemistry, Jilin University, Changchun 130012, P.R. China

# 1. EXPERIMENTAL SECTIONS

## 1.1 Synthesis of symbiotic hetero-composite $CaCl_2$/rutile $TiO_2$

A certain volume of $TiCl_4$ was dropped in 60 mL distilled water under stirring at room temperature. After stirring for 2 h, the aqueous solution was transferred to a 100 mL Teflon-lined stainless steel autoclave for hydrothermal reaction at 120 $^{o}$C for 2 h. When the reaction was completed, the precipitates were washed for several times. The final product was obtained after drying in air at 60 $^{o}$C. Product obtained when involving 13 mL $TiCl_4$ in the starting materials was labeled as $CaCl_2$/rutile $TiO_2$.

## 1.2 Synthesis of rutile reference

We calcined sample $CaCl_2$/rutile $TiO_2$ at 200 and 400 $^{o}$C in air for 2 h in a tube furnace at a heating rate of 5 K min$^{-1}$, respectively, to provide references for monitoring the structural evolution of $CaCl_2$/rutile $TiO_2$. The calcined products were named as $CaCl_2$/rutile-200 and $CaCl_2$/rutile-400, based on the calcination temperature. Commercial rutile $TiO_2$ was selected as another reference rutile $TiO_2$, labeled as Ref. rutile.

## 2.3 Sample characterization

Sample structures were characterized by X-ray diffraction (XRD) on a Rigaku MiniFlex II benchtop X-ray diffractometer using a Cu target. Al powders serve as an internal standard for peak position determination. The lattice parameters were measured by a least-squares method using GSAS software. Morphology and size information were examined by transmission electron microscope (TEM) using FEI Tecnai G2 S-Twin F20 with an acceleration voltage of 200 kV and field-emission scanning electron microscopy (SEM) (JEOL, model JSM-6700F). Samples for TEM were prepared by dispersing a powder in ethanol and leaving a droplet of suspension on a copper microscope grid covered with perforated carbon. UV-vis diffuses reflectance spectra of the samples were recorded on a Shimadzu U-4100 UV-vis-near infrared spectrometer in the range of 200-800 nm with $Al_2O_3$ as the background. Raman spectra were recorded on a Renishaw Micro-Raman system equipped with a laser of 532 nm. Brunauer−Emmett−Teller (BET) surface areas of the samples were obtained by $N_2$ adsorption/desorption isotherm performed using an apparatus of Micromeritics ASAP 2020plus.

Valence band positions of the samples were detected by X-ray photoelectron spectra (XPS), a Thermo ESCALAB 250Xi electron energy spectrometer using Al-Kα (1486.6 eV) as X-ray excitation source. X-ray absorption fine structure (XAFS) data for Ti-K edge were collected at 1W1B beamline in Beijing Synchrotron Radiation Facility (BSRF). Ti L-edge was collected at XMCD station in National Synchrotron Radiation Laboratory (NSRL), Hefei, China. Electron spin resonance (ESR) spectra were obtained using a JES-FA200 spectrometer at room temperature.

Density of states (DOS) were performed with density functional theory using the Cambridge Sequential Total Energy Package (CASTEP) program package. Electrochemical Impedance Spectroscopy (EIS) were conducted using a conventional three-electrode cell electrochemical workstation. Ag/AgCl and Pt foil (2 x 2) were used as the reference electrode and counter electrode, respectively. The working electrodes (FTO) were prepared by dropping 300 μL suspension liquid obtained through mixing 4 mg of the sample, 450 μL de-ionized water, 500 μL ethanol and 50 μL 5% Nafion solution. Microwave absorption measurements were performed using vector network analyzer (3672) at microwave frequencies of 1–18 GHz. The samples were mixed in melting paraffin wax and cast to a ring mold with thickness of 2 mm, inner diameter of 3 mm, and outer diameter of 7 mm. The content of sample was 60 wt%.

### 2.4 Photocatalytic Measurements

Photocatalytic $H_2$ evolution was carried out in a closed quartz vessel with a rubber septum. 50 mg of powders were dispersed in 50 mL aqueous solution that contains 5 mL methanol, which was vacuumed to remove air prior to light illumination. 0.15 mL $H_2PtCl_6$ solution (0.01 mol/L) was added for forming cocatalyst (1% Pt) before degassing. The mixture was irradiated by a xenon lamp (300 W) with a 400 nm cut off or an AM 1.5 G filter under continuous stirring. The evolved $H_2$ was analyzed by gas chromatography (GC-7900, Ar carrier gas, Shanghai Tianmei).

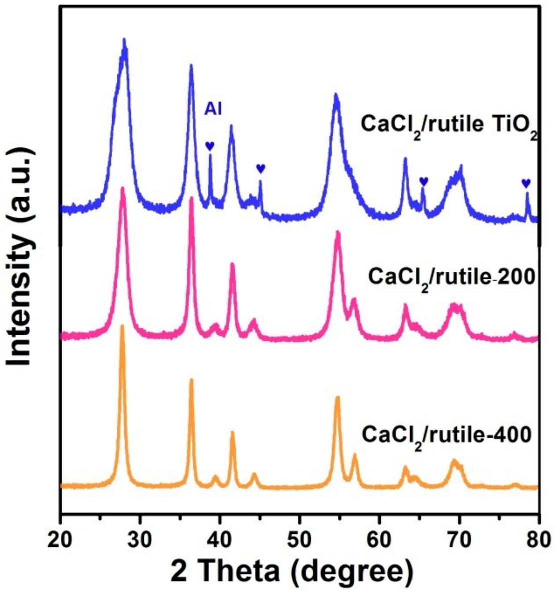

Figure S1. XRD patterns for $CaCl_2$/rutile $TiO_2$, $CaCl_2$/rutile-200, and $CaCl_2$/rutile-400.

Equation S1: $\frac{1}{d^2} = \frac{(h^2 + k^2)}{a^2} + \frac{l^2}{c^2}$

Table S1. Lattice parameters calculated from peak 1 and peak 2 of $CaCl_2$/rutile $TiO_2$ using Gaussian Fitting.

| peak | d (Å) | a (Å) | b (Å) | c (Å) | V ($Å^3$) | Size (nm) |
|---|---|---|---|---|---|---|
| Peak1 | 3.29 | 4.65 | 4.65 | 2.91 | 62.92 | 5.3 |
| Peak2 | 3.17 | 4.48 | 4.48 | 2.80 | 56.20 | 6.1 |

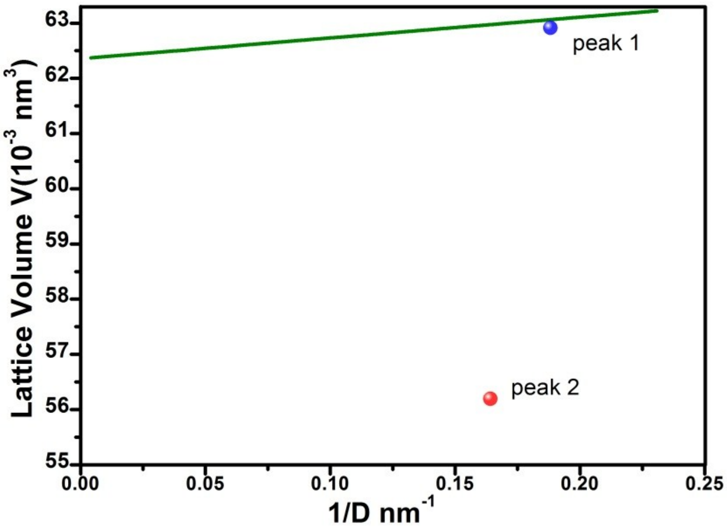

Figure S2. Relationship between 1/D and lattice volume (V) of rutile nanoparticles from reference.[1,2] Blue dot is the value calculated from the former (110) and (101) peaks. The red dot is the value calculated from the later (110) and (101) peaks.

Table S2. XRD standard data for $CaCl_2$ type structure $TiO_2$ in $CaCl_2$/rutile $TiO_2$ obtained from GSAS refinement.

| number | 2theta | d-spacing | F | h | k | l |
|---:|---:|---:|---:|---:|---:|---:|
| 1 | 27.853 | 3.2006 | 35.04 | 1 | 1 | 0 |
| 2 | 35.885 | 2.5005 | 20.95 | 1 | 0 | 1 |
| 3 | 36.096 | 2.4863 | 25.33 | 0 | 1 | 1 |
| 4 | 39.409 | 2.2846 | 14.05 | 2 | 0 | 0 |
| 5 | 40.185 | 2.2422 | 9.19 | 0 | 2 | 0 |
| 6 | 41.307 | 2.1839 | 19.75 | 1 | 1 | 1 |
| 7 | 44.469 | 2.0357 | 14.6 | 2 | 1 | 0 |
| 8 | 44.999 | 2.0129 | 7.91 | 1 | 2 | 0 |
| 9 | 54.503 | 1.6823 | 28.61 | 2 | 1 | 1 |
| 10 | 54.959 | 1.6694 | 31.99 | 1 | 2 | 1 |
| 11 | 57.548 | 1.6003 | 35.37 | 2 | 2 | 0 |
| 12 | 62.085 | 1.4938 | 39.16 | 0 | 0 | 2 |
| 13 | 64.569 | 1.4422 | 20.95 | 3 | 1 | 0 |
| 14 | 65.665 | 1.4207 | 20.26 | 1 | 3 | 0 |
| 15 | 66.194 | 1.4107 | 4.23 | 2 | 2 | 1 |
| 16 | 69.177 | 1.3569 | 35.28 | 3 | 0 | 1 |
| 17 | 69.372 | 1.3536 | 23.98 | 1 | 1 | 2 |
| 18 | 70.37 | 1.3368 | 30.55 | 0 | 3 | 1 |
| 19 | 72.755 | 1.2988 | 4.22 | 3 | 1 | 1 |
| 20 | 73.793 | 1.283 | 8.99 | 1 | 3 | 1 |
| 21 | 75.381 | 1.2599 | 1.76 | 3 | 2 | 0 |
| 22 | 76.022 | 1.2509 | 6.88 | 2 | 3 | 0 |
| 23 | 76.067 | 1.2502 | 13.42 | 2 | 0 | 2 |
| 24 | 76.578 | 1.2432 | 10.8 | 0 | 2 | 2 |
| 25 | 79.526 | 1.2043 | 8.07 | 2 | 1 | 2 |
| 26 | 79.905 | 1.1996 | 4.4 | 1 | 2 | 2 |

Table S3. XRD standard data for rutile phase $TiO_2$ in $CaCl_2$/rutile $TiO_2$ obtained from GSAS refinement.

| number | 2theta | d-spacing | F | h | k | l |
|---|---|---|---|---|---|---|
| 1 | 27.144 | 3.2826 | 35.8 | 1 | 1 | 0 |
| 2 | 36.071 | 2.488 | 22.69 | 0 | 1 | 1 |
| 3 | 38.764 | 2.3211 | 11.61 | 0 | 2 | 0 |
| 4 | 41.13 | 2.1929 | 19.78 | 1 | 1 | 1 |
| 5 | 43.559 | 2.0761 | 12.16 | 1 | 2 | 0 |
| 6 | 53.984 | 1.6972 | 30.58 | 1 | 2 | 1 |
| 7 | 55.981 | 1.6413 | 36.04 | 2 | 2 | 0 |
| 8 | 63.037 | 1.4735 | 38.72 | 0 | 0 | 2 |
| 9 | 63.299 | 1.468 | 20.19 | 1 | 3 | 0 |
| 10 | 64.988 | 1.4339 | 5.28 | 2 | 2 | 1 |
| 11 | 68.423 | 1.37 | 34.19 | 0 | 3 | 1 |
| 12 | 69.924 | 1.3443 | 24.12 | 1 | 1 | 2 |
| 13 | 71.779 | 1.314 | 6.61 | 1 | 3 | 1 |
| 14 | 73.493 | 1.2875 | 4.17 | 2 | 3 | 0 |
| 15 | 76.518 | 1.244 | 12.18 | 0 | 2 | 2 |
| 16 | 79.743 | 1.2016 | 6.58 | 1 | 2 | 2 |
| 17 | 81.519 | 1.1798 | 13.41 | 2 | 3 | 1 |
| 18 | 83.17 | 1.1606 | 23.22 | 0 | 4 | 0 |
| 19 | 86.339 | 1.1259 | 9.6 | 1 | 4 | 0 |
| 20 | 89.263 | 1.0964 | 25.98 | 2 | 2 | 2 |
| 21 | 89.496 | 1.0942 | 26.66 | 3 | 3 | 0 |
| 22 | 76.022 | 1.2509 | 6.88 | 2 | 3 | 0 |
| 23 | 76.067 | 1.2502 | 13.42 | 2 | 0 | 2 |
| 24 | 76.578 | 1.2432 | 10.8 | 0 | 2 | 2 |
| 25 | 79.526 | 1.2043 | 8.07 | 2 | 1 | 2 |
| 26 | 79.905 | 1.1996 | 4.4 | 1 | 2 | 2 |

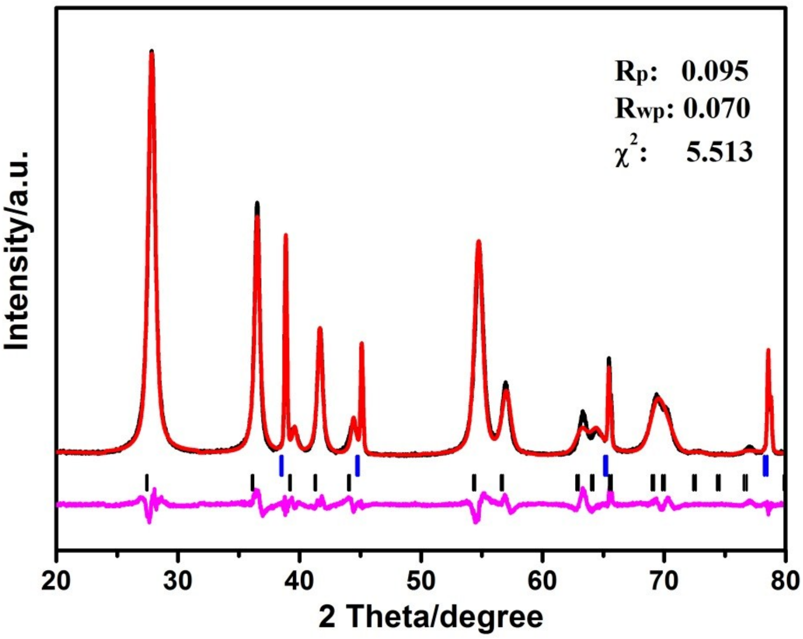

Figure S3. XRD for $CaCl_2$/rutile-400. The black, red, and pink curves are experimental diffraction data, calculated data, and deviation between the experimental and calculated values, respectively. The blue and black vertical data are standard diffraction lines for internal standard Al and rutile $TiO_2$, respectively.

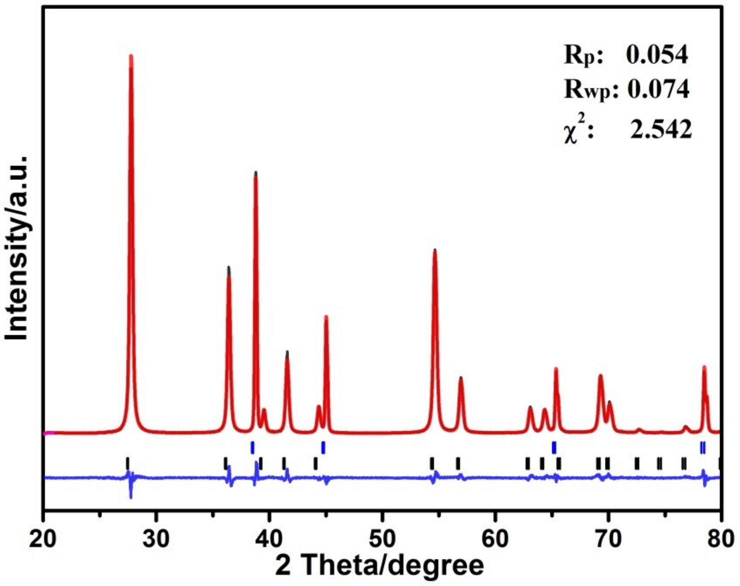

Figure S4. XRD for commercial rutile $TiO_2$. The black, red, and blue curves are experimental diffraction data, calculated data, and deviation between the experimental and calculated value respectively. The blue and black vertical data are standard diffraction lines for internal standard Al and rutile $TiO_2$, respectively.

Table S4. XRD standard data for rutile phase $TiO_2$ in $CaCl_2$/rutile-400 obtained from GSAS refinement.

| number | 2theta | d-spacing | F | h | k | l |
|---|---|---|---|---|---|---|
| 1 | 27.42 | 3.2501 | 35.54 | 1 | 1 | 0 |
| 2 | 36.092 | 2.4866 | 22.94 | 0 | 1 | 1 |
| 3 | 39.167 | 2.2981 | 11.38 | 0 | 2 | 0 |
| 4 | 41.245 | 2.1871 | 19.88 | 1 | 1 | 1 |
| 5 | 44.017 | 2.0555 | 11.76 | 1 | 2 | 0 |
| 6 | 54.312 | 1.6877 | 30.41 | 1 | 2 | 1 |
| 7 | 56.591 | 1.625 | 36.12 | 2 | 2 | 0 |
| 8 | 62.807 | 1.4783 | 38.82 | 0 | 0 | 2 |
| 9 | 64.007 | 1.4535 | 20.28 | 1 | 3 | 0 |
| 10 | 65.49 | 1.4241 | 4.95 | 2 | 2 | 1 |
| 11 | 68.981 | 1.3603 | 33.75 | 0 | 3 | 1 |
| 12 | 69.84 | 1.3457 | 24.05 | 1 | 1 | 2 |
| 13 | 72.392 | 1.3044 | 6.88 | 1 | 3 | 1 |
| 14 | 74.352 | 1.2748 | 4.19 | 2 | 3 | 0 |
| 15 | 76.568 | 1.2433 | 12.02 | 0 | 2 | 2 |
| 16 | 79.856 | 1.2002 | 6.41 | 1 | 2 | 2 |

Table S5. XRD standard data for rutile phase $TiO_2$ in commercial rutile $TiO_2$ obtained from GSAS refinement.

| number | 2theta | d-spacing | F | h | k | l |
|---:|---:|---:|---:|---:|---:|---:|
| 1 | 27.437 | 3.2481 | 35.72 | 1 | 1 | 0 |
| 2 | 36.086 | 2.487 | 22.69 | 0 | 1 | 1 |
| 3 | 39.192 | 2.2968 | 11.67 | 0 | 2 | 0 |
| 4 | 41.246 | 2.187 | 19.74 | 1 | 1 | 1 |
| 5 | 44.045 | 2.0543 | 12.04 | 1 | 2 | 0 |
| 6 | 54.327 | 1.6873 | 30.47 | 1 | 2 | 1 |
| 7 | 56.629 | 1.624 | 35.77 | 2 | 2 | 0 |
| 8 | 62.774 | 1.479 | 38.84 | 0 | 0 | 2 |
| 9 | 64.051 | 1.4526 | 20.08 | 1 | 3 | 0 |
| 10 | 65.516 | 1.4236 | 5.23 | 2 | 2 | 1 |
| 11 | 69.011 | 1.3598 | 33.97 | 0 | 3 | 1 |
| 12 | 69.817 | 1.346 | 24.14 | 1 | 1 | 2 |
| 13 | 72.425 | 1.3039 | 6.55 | 1 | 3 | 1 |
| 14 | 74.404 | 1.274 | 4.12 | 2 | 3 | 0 |
| 15 | 76.554 | 1.2435 | 12.17 | 0 | 2 | 2 |
| 16 | 79.846 | 1.2003 | 6.57 | 1 | 2 | 2 |
| 17 | 82.344 | 1.1701 | 13.36 | 2 | 3 | 1 |
| 18 | 84.254 | 1.1484 | 23.03 | 0 | 4 | 0 |
| 19 | 87.485 | 1.1141 | 9.47 | 1 | 4 | 0 |
| 20 | 89.567 | 1.0935 | 25.92 | 2 | 2 | 2 |

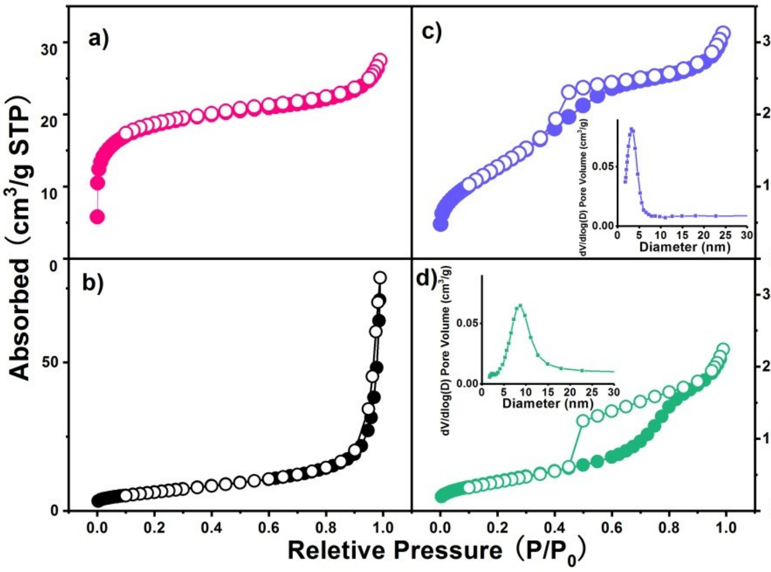

Figure S5. Nitrogen adsorption/desorption isotherms of a) $CaCl_2$/rutile $TiO_2$, b) commercial rutile $TiO_2$, c) $CaCl_2$/rutile-200, and d) $CaCl_2$/rutile-400. Inserts are their pore size distribution curves.

Table S6. Specific surface areas for $CaCl_2$/rutile $TiO_2$, $CaCl_2$/rutile -200, $CaCl_2$/rutile -400, and commercial rutile $TiO_2$ (*Ref.rutile*).

| sample | $CaCl_2$/rutile $TiO_2$ | $CaCl_2$/rutile -200 | $CaCl_2$/rutile -400 | *Ref.rutile* |
|---|---|---|---|---|
| BET($m^2/g$) | 59.6 | 48.1 | 15.3 | 23.5 |

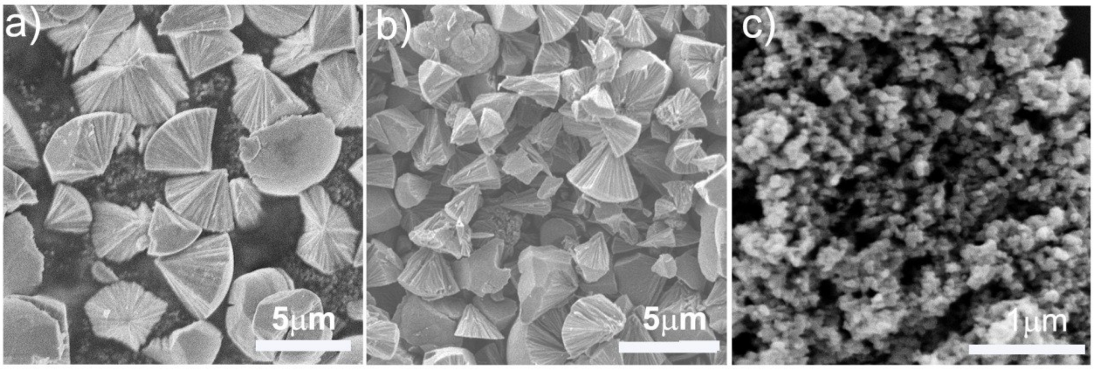

Figure S6. SEM images of a) $CaCl_2$/rutile $TiO_2$, b) $CaCl_2$/rutile-400, and c) commercial rutile $TiO_2$ (Ref.rutile).

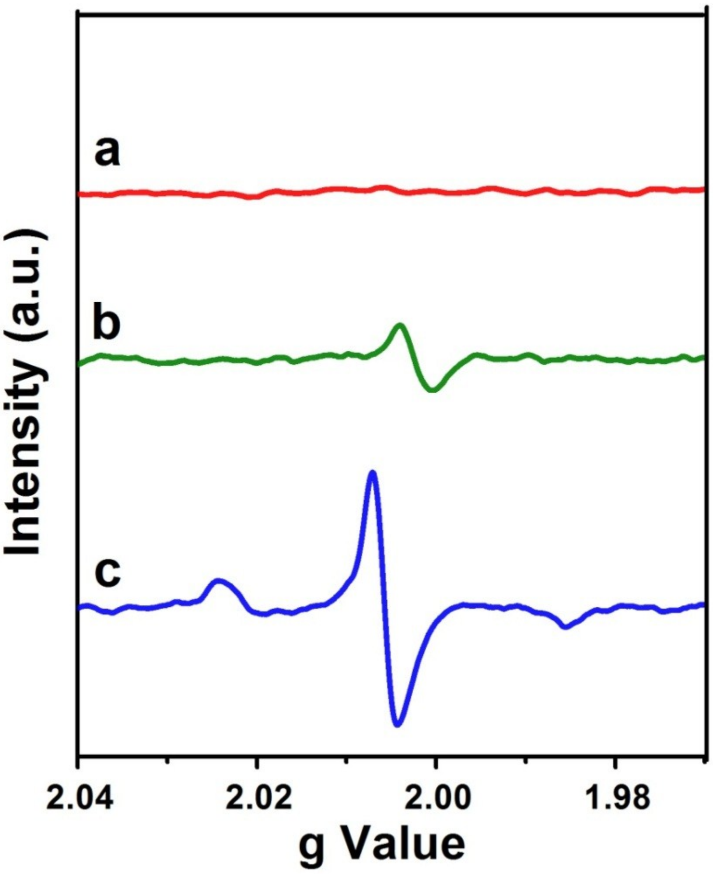

Figure S7. Electron spin resonance (ESR) spectra of $CaCl_2$/rutile $TiO_2$, $CaCl_2$/rutile-200, and $CaCl_2$/rutile-400.

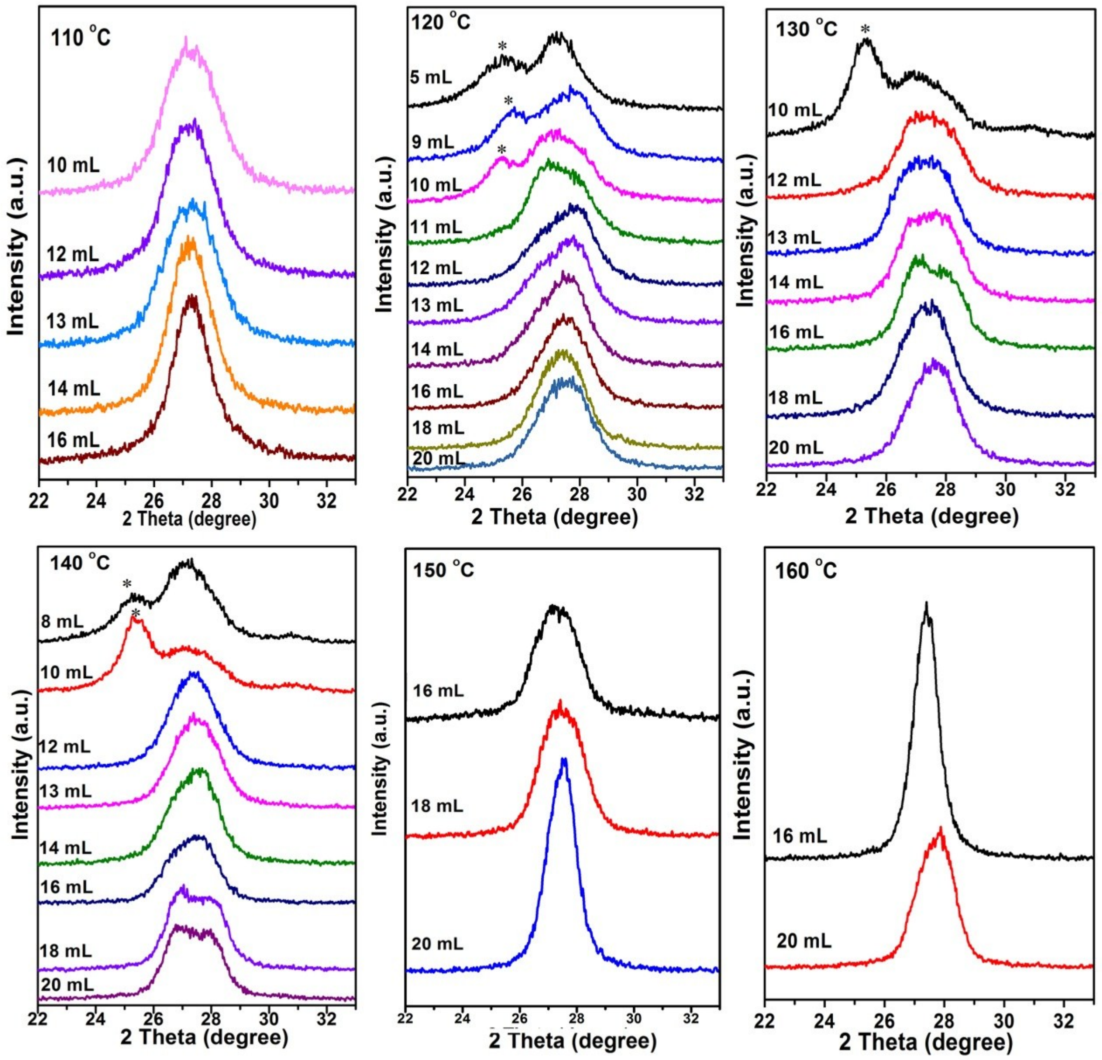

Figure S8. XRD patterns for the products obtained at different hydrothermal temperatures (110-160 °C) and addition amounts of $TiCl_4$ (5-20 mL).

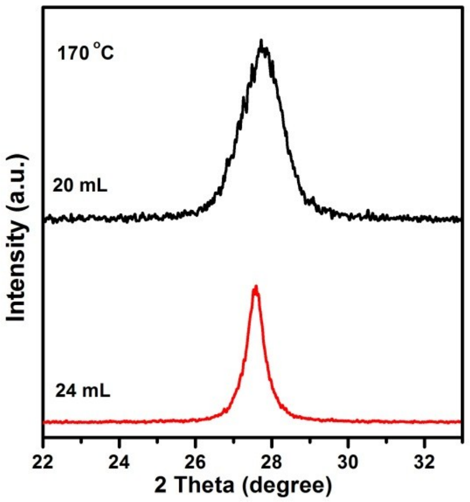

Figure S9. XRD patterns for the products obtained using given amounts of $TiCl_4$ (20 mL and 24 mL) at a fixed hydrothermal temperature of 170 °C.

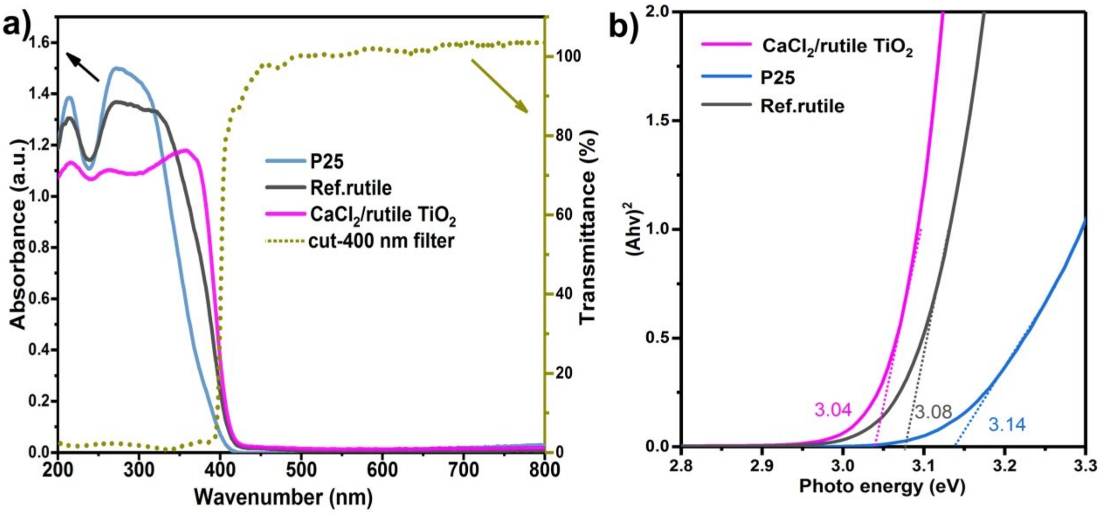

Figure S10. a) Diffuse reflectance ultraviolet-visible spectra and b) converted diagram using function $(\alpha h\nu)^n = k(h\nu - E)$. The short dotted line in a) is the light transmittance of cut-400 nm filter used in photocatalytic reactions.

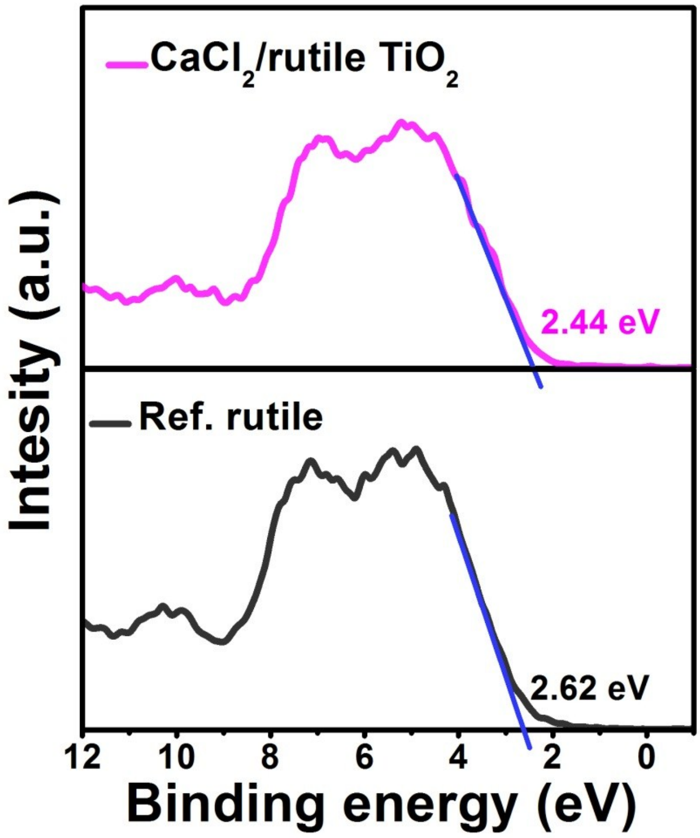

Figure S11. XPS valence band spectra for $CaCl_2$/rutile $TiO_2$ and commercial rutile $TiO_2$ (Ref.rutile).

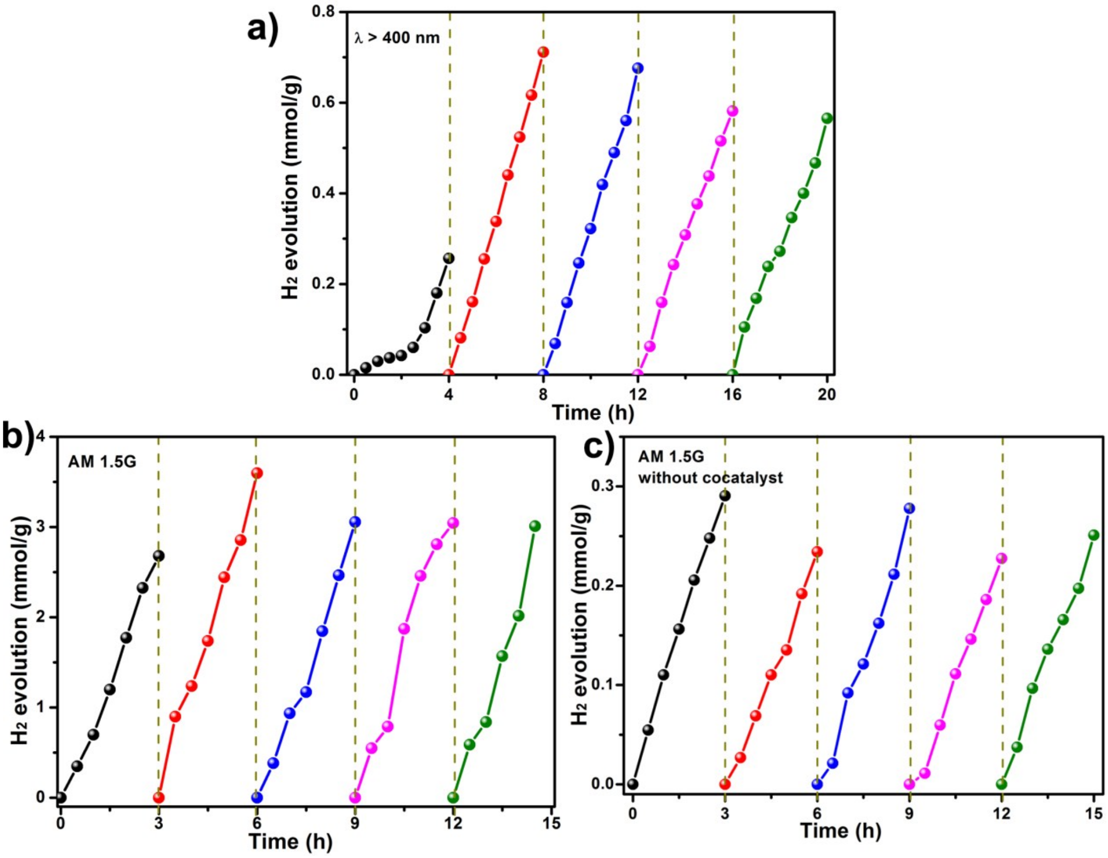

Figure S12. The cyclic stability of $CaCl_2$/rutile $TiO_2$ for photocatalytic $H_2$ generation under a) visible light ( λ >400 nm), b) AM 1.5G with and d) without cocatalyst Pt.

The cyclic stability of $CaCl_2$/rutile $TiO_2$ for photocatalytic $H_2$ generation under visible light (λ>400 nm), AM 1.5G with and without cocatalyst of Pt were presented in Figure S12. It is shown that $CaCl_2$/rutile $TiO_2$ exhibited an excellent stability in photocatalytic process. When a cocatalyst Pt was added, the activity of photocatalytic $H_2$ generation for the first cycle was low when compared to the following cycles due to the Pt deposition and activation process. This phenomenon is obvious under the illumination of visible light (λ>400 nm), which may be due to the weak ability for catalyst to absorb light in this range. Thus, Pt deposition process will be longer.

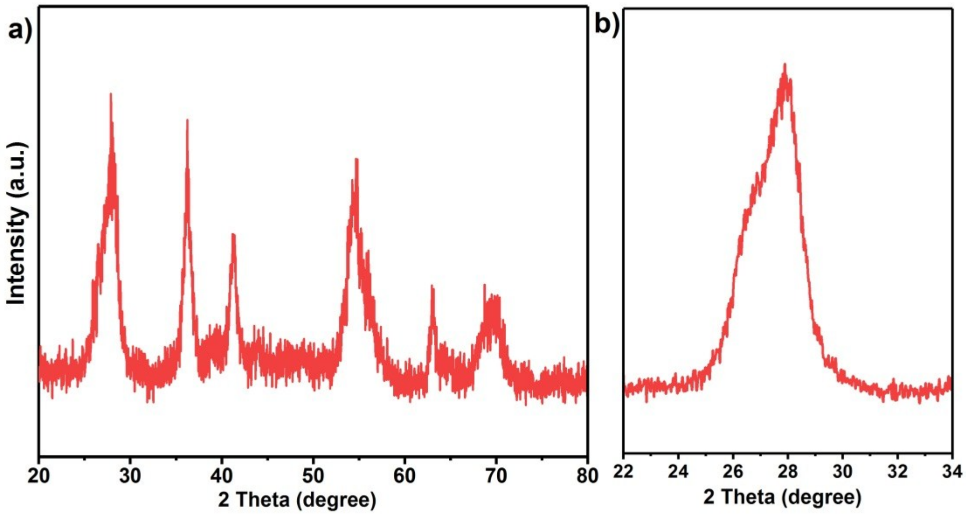

Figure S13. a) XRD pattern and b) enlarged pattern for the sample after visible light photocatalytic test.

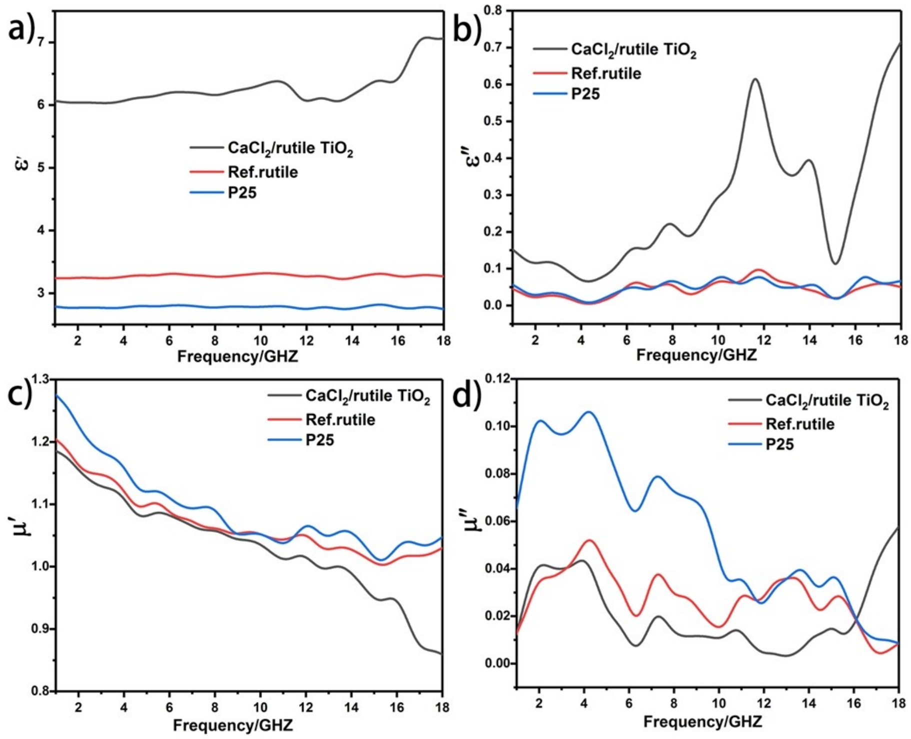

Figure S14. Frequency dependence of a) the real part, μ′ and b) the imaginary part, μ″ of the complex permittivity, c) the real par, ε′ and d) the imaginary part, ε″ of the complex permeability of $CaCl_2$/rutile $TiO_2$, Ref.$TiO_2$ and P25.

Microwave absorption properties were evaluated with the complex permittivity (the real part:ε′, the imaginary part: ε″) and permeability (the real part:μ′, the imaginary part: μ″) values of $CaCl_2$/rutile $TiO_2$, commercial rutile (Ref. $TiO_2$) and P25. ε′ and ε″ are related to the storage and dissipation (or loss) of electrical energy. μ′ and μ″ are related to the storage and dissipation (or loss) of magnetic energy. As presented in Figure S14, compared with Ref.$TiO_2$ and P25, $CaCl_2$/rutile $TiO_2$ showed the highest ε′ and ε″ in the frequency range of 1-18 GHZ. It indicates that $CaCl_2$/rutile $TiO_2$ is more efficient in dissipating the electrical energy under the electromagnetic field. Meanwhile, the μ′ of $CaCl_2$/rutile $TiO_2$ was higher than that of Ref.$TiO_2$ and P25 in the region of 1-18 GHZ. The μ″of $CaCl_2$/rutile $TiO_2$ was lower than that of Ref.$TiO_2$ and P25 in the frequency range of 1-16 GHZ and higher in the frequency ranges of 16-18 GHZ. The changes of the ε′, ε″, μ′ and μ″ value of $CaCl_2$/rutile $TiO_2$ were likely from the existence of $CaCl_2$ phase $TiO_2$.

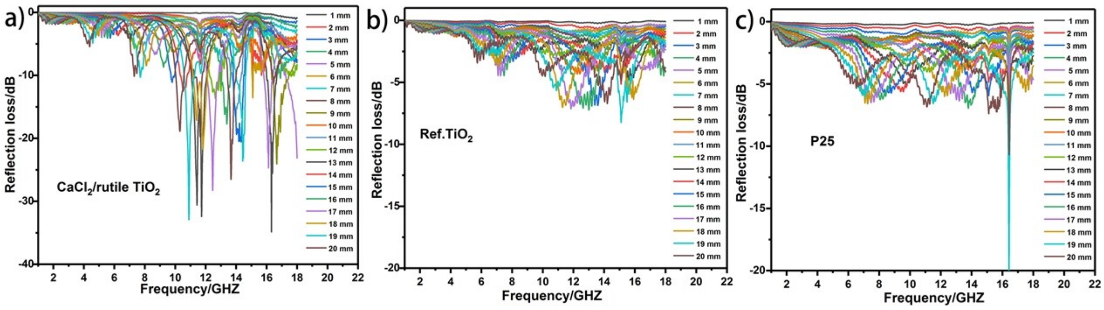

Figure S15. Frequency dependence of the reflection loss of a) $CaCl_2$/rutile $TiO_2$, b) Ref.$TiO_2$ and c) P25.

The reflection loss curve can be calculated based on the complex permittivity and permeability parameters according to the equations reported previously.[2] Thus, frequency dependence of reflection loss for all samples with different thickness (1-20 mm) was obtained (Figure S15). Obviously, compared with Ref.$TiO_2$ and P25, $CaCl_2$/rutile $TiO_2$ showed the highest reflection loss. Even so, a material with a reflection loss value less than -30 dB is regarded as an excellent absorber and $CaCl_2$/rutile $TiO_2$ can have such a value once the thickness is very big. Hydrogenation had been found to be a good approach to enhance the microwave property. Thus, if this material is to be used in microwave absorption, further work is highly needed on structural modification.

Reference

1. W. B. Hu, L. P. Li, W. M. Tong, G. S. Li and T. J. Yan, *Journal of Materials Chemistry*, 2010, **20**, 8659-8667.
2. G. Li, J. Boerio-Goates, B. F. Woodfield and L. Li, Applied Physics Letters, 2004, 85, 2059-2061.
3. L. Tian, X. Yan, J. Xu, P. Wallenmeyer, J. Murowchick, L. Liu and X. Chen, J. *Mater. Chem. A,* 2015, **3,** 12550-12556.